Supplement of Atmos. Chem. Phys., 26, 13595–13615, 2026
https://doi.org/10.5194/acp-26-13595-2026-supplement

Atmospheric Chemistry and Physics
Open Access

Supplement of

Origin of low ozone above western North America: an investigation of sources and trends

Ju-Mee Ryoo et al.

Correspondence to: Ju-Mee Ryoo (ju-mee.ryoo@nasa.gov)

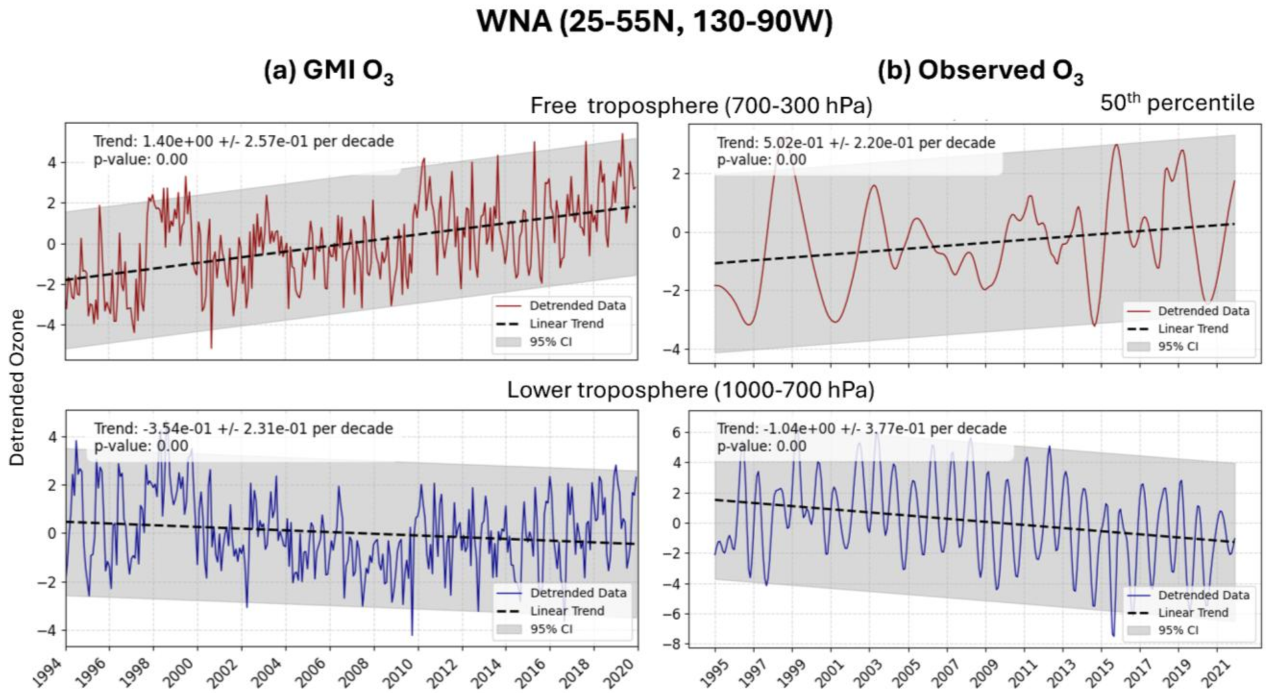

Figure S1. Increase in free tropospheric ozone (O_3) and decrease in surface O_3 over western North America (WNA; 25–55°N, 130–90°W): Time series of monthly mean layer-averaged O_3 anomaly in (a) the free troposphere (700–300 hPa) and (b) the lower tropospheric layer (1000–850 hPa) over WNA. Data are obtained from (left) GMI from 1994-2019 and (right) surface and aircraft observations of 50th percentile of O_3 from 1995-2021 (see more details in Chang et al., 2023a). The trend with uncertainty (± 2 standard errors) and *p*-values are shown in the plot, respectively.

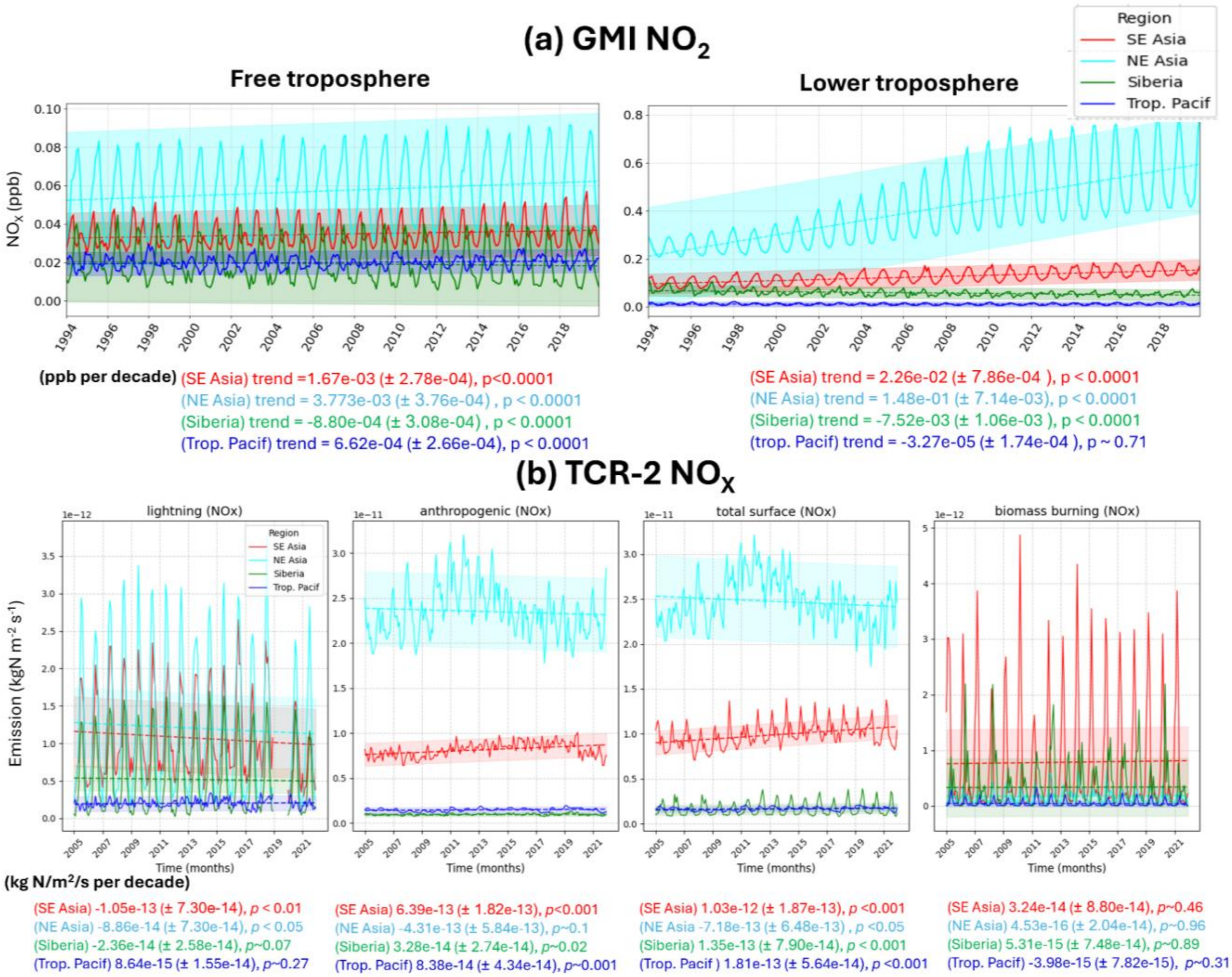

Figure S2. NO_x trends derived from chemical reanalysis products from two different dataset: (a) The trend (lines, ppb/decade) with uncertainty (± 2 standard errors) in GMI NO_2 concentrations in both free troposphere and lower troposphere (1000–700 hPa) from 1994 to 2019. (b) TCR-2 lightning, anthropogenic, surface, and biomass burning NO_x emissions (kg N m^{-2} s^{-1}) averaged over for different source regions (SE Asia, NE Asia, Siberia, and Tropical Pacif) from 2005 to 2022.

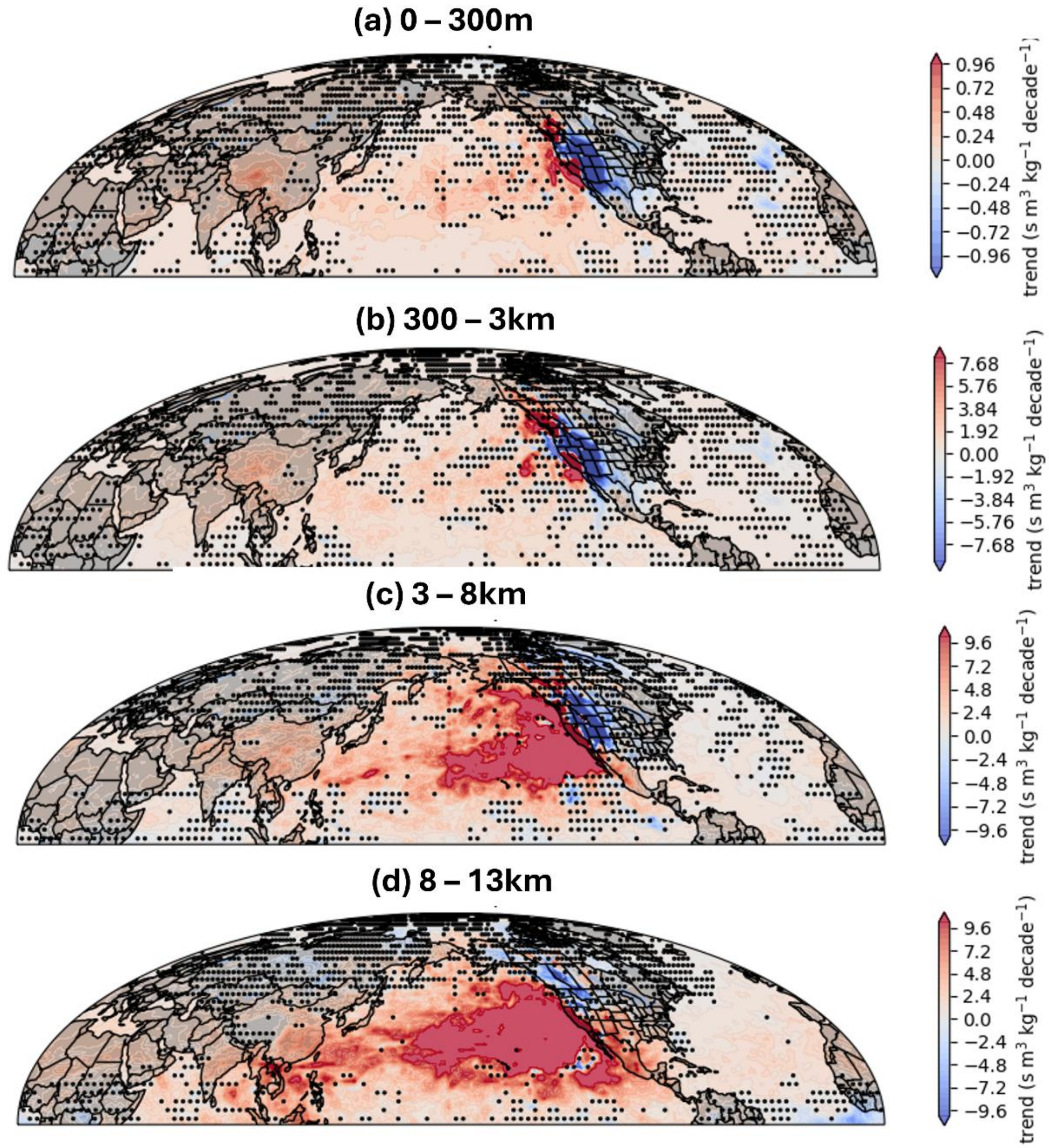

Figure S3. Trends in SRR (s m^3 kg^{-1} $decade^{-1}$): SRR trends for high O_3 levels ($66^{th} < O_3 < 95^{th}$ percentile) over WNA across the following altitude ranges: (a) 0–300 m, (b) 300 m–3 km, (c) 3–8 km, and (d) 8–13 km. The dots on the maps represent the grid cells with a low confidence value (*p-value* ≥ 0.05).

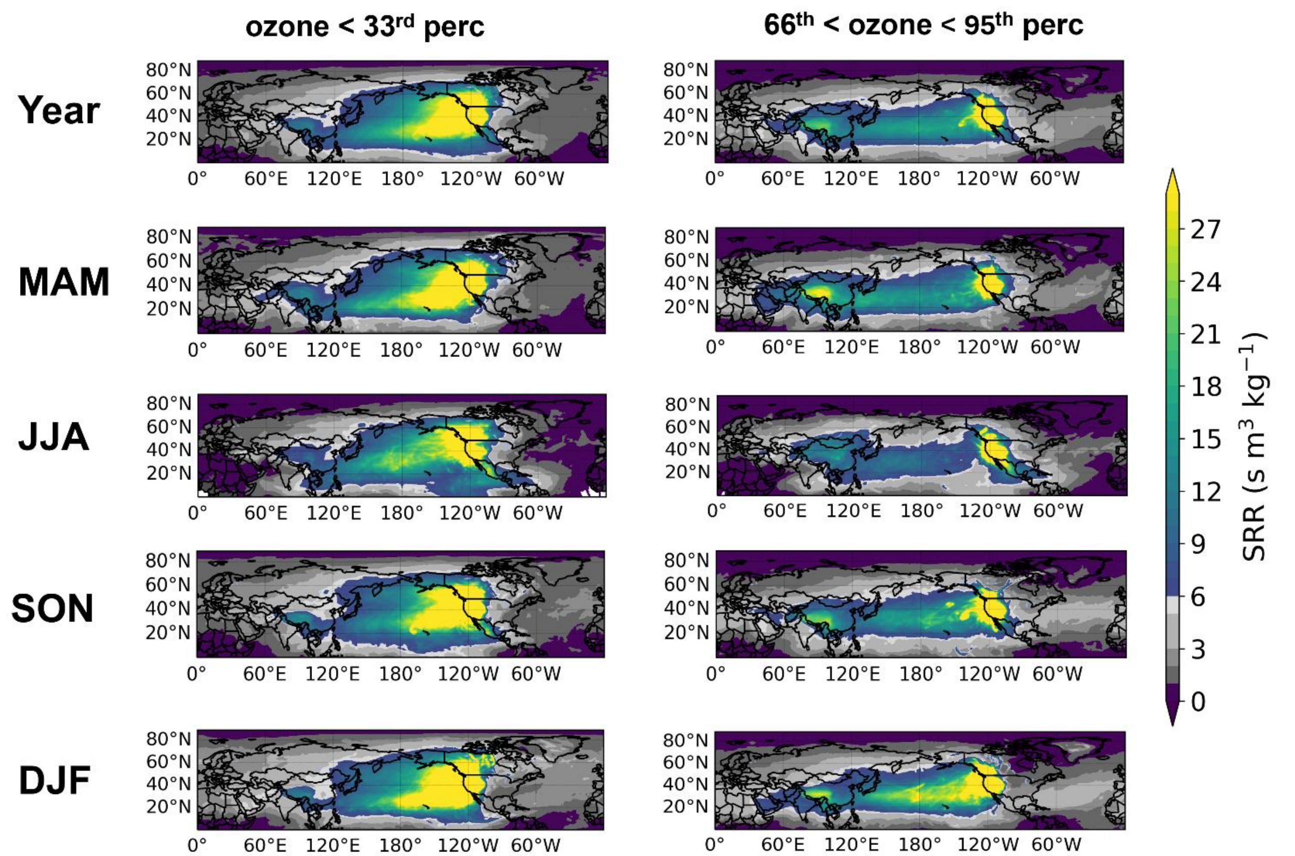

Figure S4. FLEXPART-ERA5 Source-Receptor Relationships (SRR, s m^3 kg^{-1}) for (left) low O_3 (< 33rd percentile) and (right) high O_3 (66th – 95th percentile) over WNA at the 300 m–3 km level, shown for (from top to bottom) the entire year, MAM (March, April, and May), JJA (June, July, and August), SON (September, October, and November), and DJF (December, January, and February), respectively.

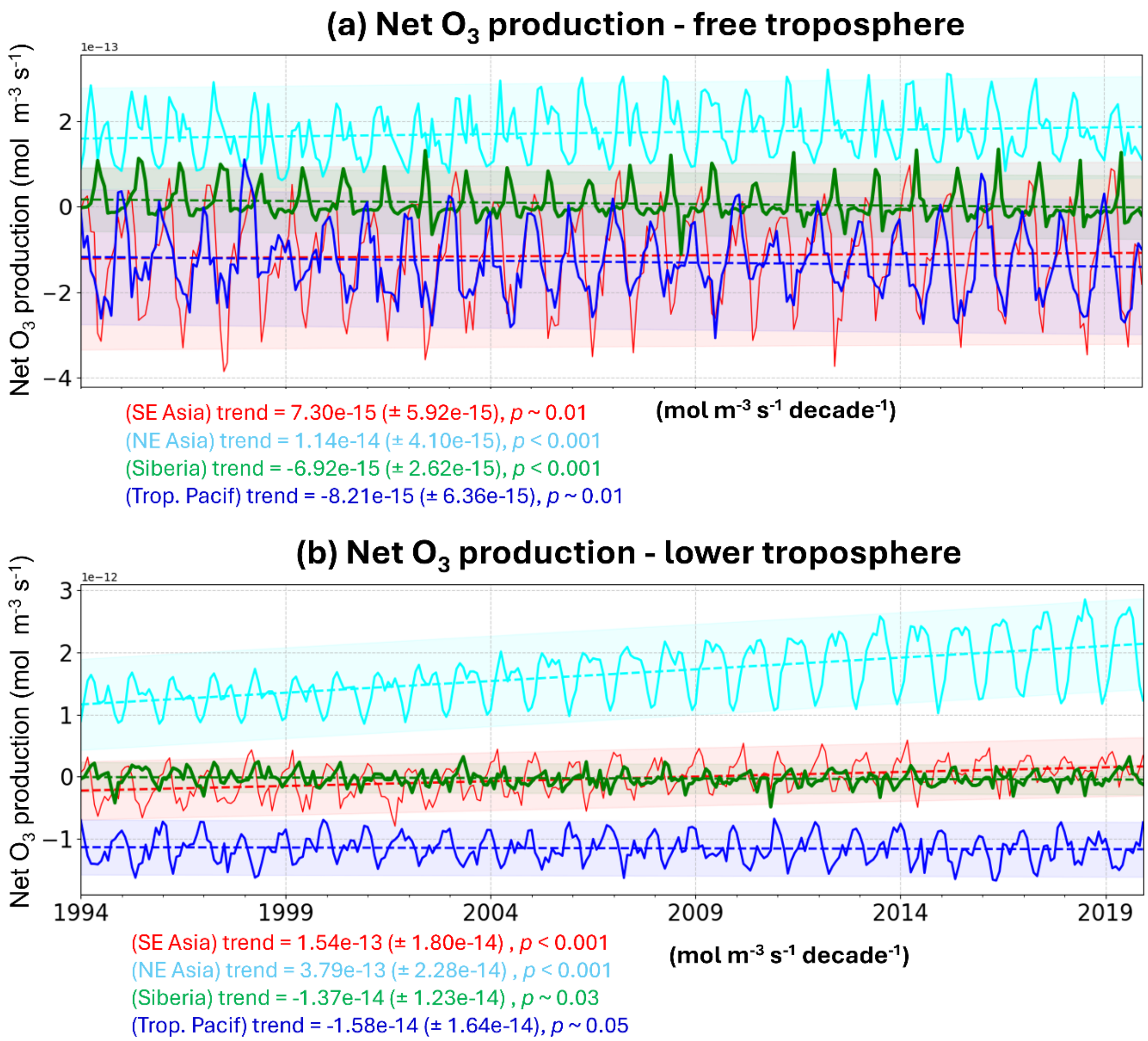

Figure S5. Net O_3 production and its trend (mol m^{-3} s^{-1} decade^{-1}) with uncertainty (± 2 standard errors) over the four source regions: SE Asia, NE Asia, Siberia, and Tropical Pacific in the (a) free troposphere (700–288.88 hPa) and (b) lower troposphere (725–985 hPa) and its trend (mol m^{-3} s^{-1} decade^{-1}) from 1994 to 2021.

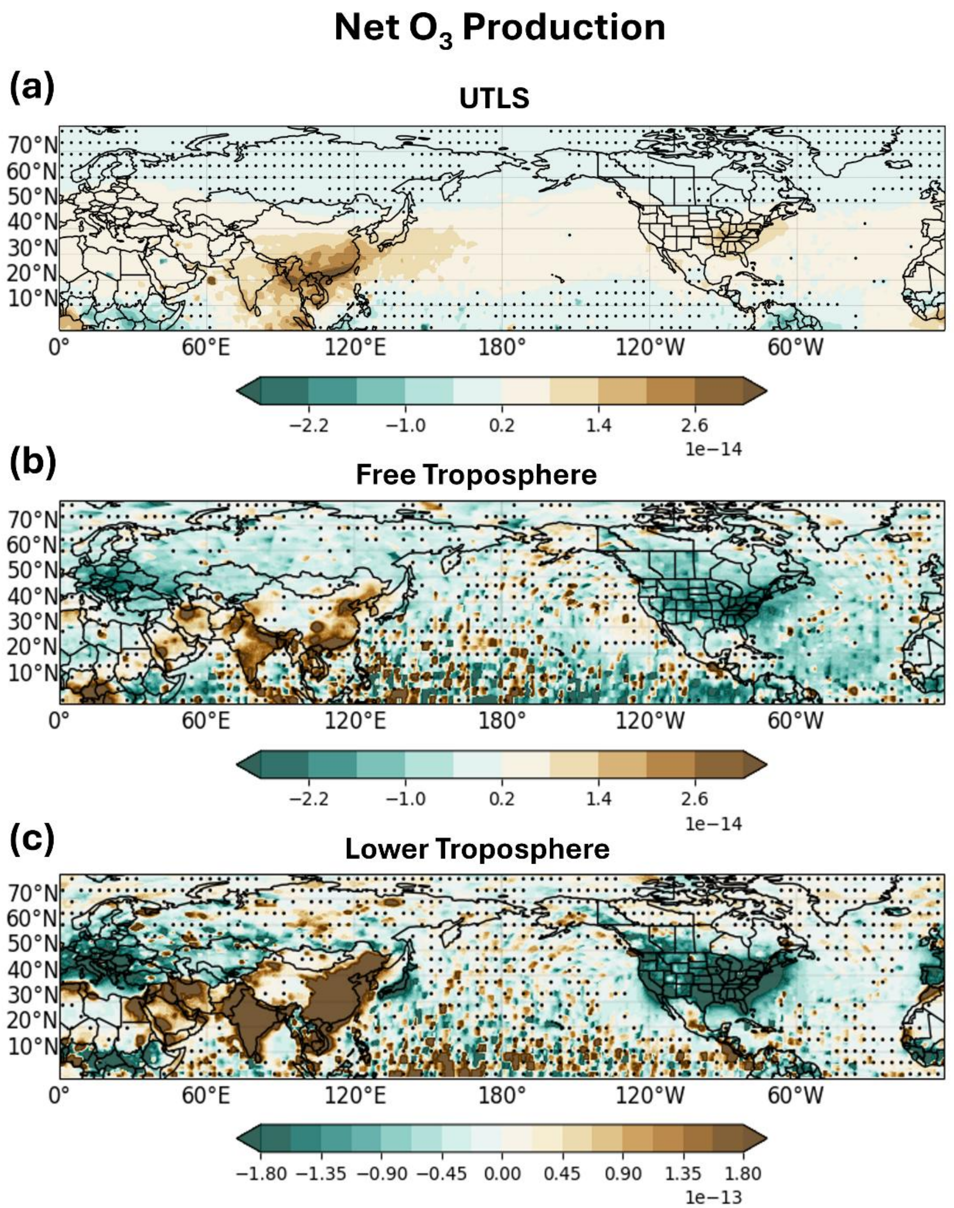

Figure S6. GMI net O_3 production trend (mol m^{-3} s^{-1} $decade^{-1}$) in the (a) UTLS (244.88–176.93 hPa) (b) free troposphere (700–288.88 hPa) and (c) lower troposphere (725–985 hPa) calculated from 1994 and 2019. The dots on the maps represent the grid cells with a low confidence value (*p-value* ≥ 0.05).

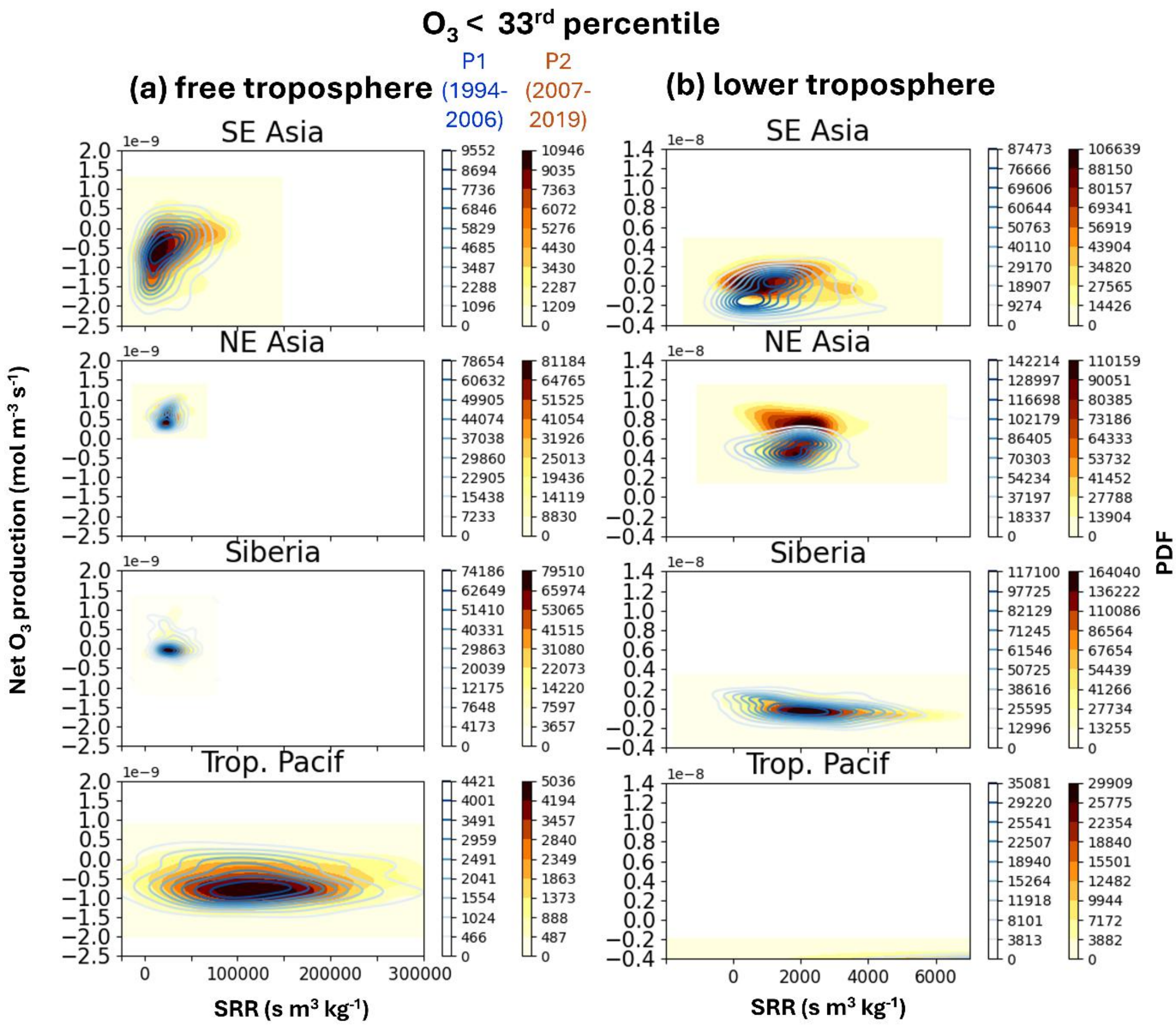

Figure S7. Distribution and relationship between SRR and O_3 net production in regions influencing low O_3 (< 33rd percentile) over WNA during the two periods (P1:1994–2006 (contour) and P2: 2007–2019 (shading)): 2-D joint PDF of the O_3 net production and monthly mean SRR over SE Asia, NE Asia, Siberia, and Tropical Pacific, for (a) free troposphere, and (b) lower troposphere.

In Figs. 6 and 8 in the main text, we demonstrate that positive net O_3 production primarily occurs over Southeast (SE) Asia and Northeast (NE) Asia in the lower and free troposphere, and across most regions in the upper troposphere and lower stratosphere (UTLS), underscoring the importance of these regions as major sources contributing to O_3 production and its downstream impacts on O_3 levels over WNA. Figure S7 further illustrates the contributions of net O_3 production to low O_3 concentrations (<33rd percentile) over WNA, as a function of SRR, categorized across the vertical layers and time periods.

SE Asia exhibits significantly higher SRR in both the UTLS and free troposphere alongside strong net O_3 production. This indicates a stronger influence on low O_3 over WNA compared to NE Asia (Fig. S7a, b). Interestingly, there's no notable difference in SRR between the two time periods—P1 (blue contours) and P2 (shading)—in the free troposphere. However, a modest increase in SRR is observed in the UTLS (not shown), consistent with patterns shown in Fig. 3. Along with this, O_3 production over SE and NE Asia has increased in both the lower and free troposphere, with particularly pronounced rise in the lower troposphere (Fig. S7a, b). This suggests that the recent increases in low O_3 levels over WNA are largely attributable to enhanced surface emissions and other sources, such as aircraft emissions, from SE Asia, combined with continued O_3 transport in the free troposphere and UTLS.

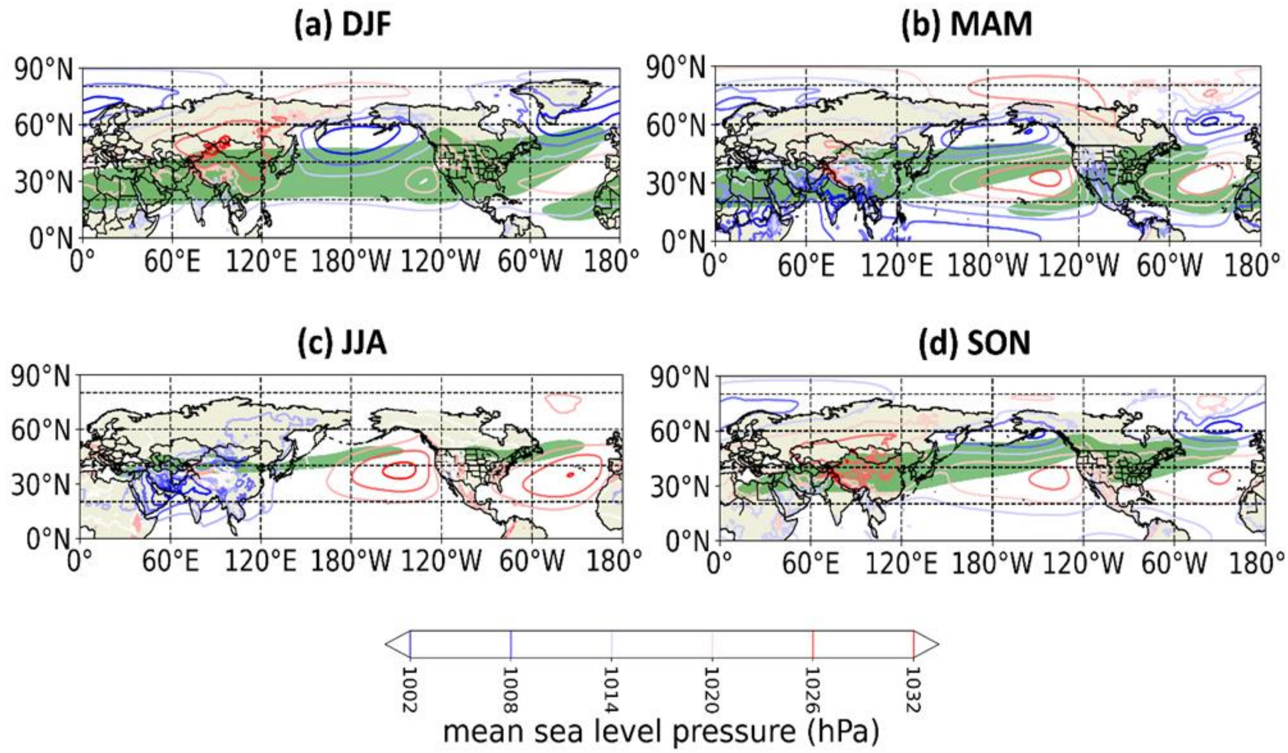

Figure S8. Climatology of the mean jet location and mean sea level pressure (MSLP) during (a) DJF, (b) MAM, (c) JJA, and (d) SON: Maps display MSLP (contours, hPa) and upper-level jet winds (green shading, m s^{-1}) based on ERA5 reanalysis data. Red contours indicate high-pressure regions, while blue contours indicate low-pressure regions. Shaded areas represent 300 hPa zonal wind speeds greater than 30 m s^{-1}.

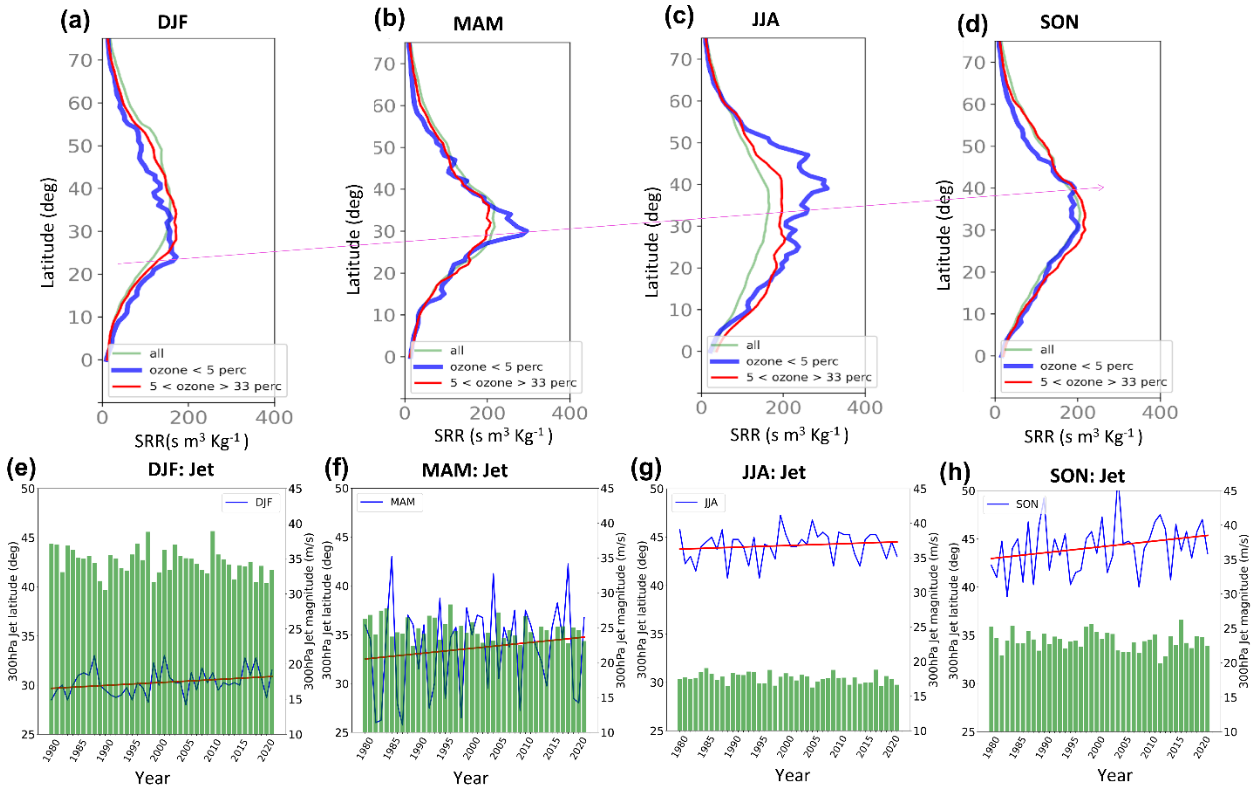

Figure S9. Seasonality of SRR and maximum upper-level jet location: (a-d) Latitudinal distribution of SRR/residence time for all O_3 levels, low O_3 levels (<5th percentile, 5th < O_3 < 33rd percentile) across the seasons: boreal winter (DJF), boreal spring (MAM), boreal summer (JJA), and boreal fall (SON). (e-h) Time series of the jet maximum location (blue line, with a red line indicating the linear regression) and its magnitude (green bars). The jet is defined as the maximum zonal wind speed at 300 hPa, with its location determined by where this maximum is observed. The figure highlights that the subtropical jet (~30°N) is dominant during boreal winter and boreal spring, while the mid-latitude (or polar) jet (~45°N) becomes dominant during boreal summer and fall.